COLLIDE-2: Collisions Into Dust Experiment-2
Final Report

November 15, 2002

Principal Investigator and Payload Manager:
Joshua E. Colwell
Laboratory for Atmospheric and Space Physics
University of Colorado
Campus Box 392
Boulder CO 80309-0392

Period of performance: January 1999-November 15, 2002

NASA Grant: NAG3-2267

The Collisions Into Dust Experiment-2 (COLLIDE-2) was the second flight of the COLLIDE payload. The payload performs six low-velocity impact experiments to study the collisions that are prevalent in planetary ring systems and in the early stages of planet formation. Each impact experiment is into a target of granular material, and the impacts occur at speeds between 1 and 100 cm/s in microgravity and in a vacuum. The experiments are recorded on digital videotape which is later analyzed.

During the period of performance a plan was developed to address some of the technical issues that prevented the first flight of COLLIDE from being a complete success, and also to maximize the scientific return based on the science results from the first flight. The experiment was modified following a series of reviews of the design plan, and underwent extensive testing. Following a brief period of storage, the experiment flew as a Hitchhiker payload on the MACH-1 Hitchhiker bridge on STS-108 in December 2001. The experiment was retrieved in January 2002, and all six impact experiments functioned nominally.

The data from the experiment show that the primary goal of identifying transition regimes for low-velocity impacts based on cratering versus accretion was achieved. These data have been analyzed and submitted for publication. That manuscript is attached to this report. Preliminary results were reported at the Lunar and Planetary Science Conference (Colwell and Mellon, 2002) and at the Sixth Microgravity Fluid Physics and Transport Phenomena Conference (Colwell et al., 2002). The experiment parameters are summarized in Table 1, and the results are summarized in Table 2.

Table 1: Experimental Parameters

IBS **Parameter**	1	2	3	4	5	6
Measured Impact Speed (cm/s)	110±10	3.60±0.1	1.29±0.01	81±10	12.2±0.1	28±2
Projectile mass (g)	10.71	9.64	10.29	8.66	8.98	10.62
Target material	Quartz Sand	Quartz Sand	Quartz Sand	Quartz Sand	JSC-1	Quartz Sand
Target bulk density (g/cm^3)	1.49	1.53	1.50	1.52	1.25	1.49
Target void ratio	0.78	0.73	0.77	0.74	1.32	0.78
Target porosity	0.44	0.42	0.43	0.43	0.57	0.44
Target Relative Density	0.07	0.23	0.12	0.18	N/M	0.09

The density of the projectiles is 2.65 g/cm^3. Both target materials were sieved to particle size ranges of 75-250 microns. The void ratio for the JSC-1 target exceeds the nominal maximum value for JSC-1 because all particles smaller than 75 microns were removed. These small particles would normally fill void spaces leading to a lower porosity. For this reason the relative density of the JSC-1 target is not measured (N/M). Uncertainties in impact speed are based on uncertainty in measuring impactor position. This is controlled by pixel size at the slowest speeds and image smear at the fastest speeds.

Table 2: Experiment Summary

IBS	Impact Speed (cm/s)		Rebound Speed (cm/s)		ε_n	Crater Diameter (cm)	Maximum Ejecta Velocity (cm/s)
	X	Y	X	Y			
1	110±10	0±2	1.10	0.85	0.01	6±2	10±1
2	0.01±0.01	3.62±0.04	0	0	0	0	0
3	1.29±0.01	0.14±0.04	0	0	0	0	0
4	81±10	0±2	1.2	0.67	0.015	N/M	16±1
5	0.12±0.06	12.15±0.1	0	0	0	0	1.5±0.2
6	24.9±2	2.4±1	0.50	0.32	0.02	4±2	3±1

Notes: Speed uncertainties are the higher of the formal 1-sigma uncertainty in the fit to the trajectory data or the uncertainty introduced by smear in the image. ε_n is the ratio of the normal component of the rebound velocity to the normal component of the impact velocity. Movement out of the X-Y plane was not measured. N/M = Not measured. Crater diameters of 0 represent impacts where the impactor embedded itself in the target without creating a detectable larger displacement of target material.

We found that our 2-cm impactors rebounded at 28 cm/s and stuck at 12 cm/s, while on the first flight of COLLIDE impactors at 17 cm/s into denser targets also rebounded. Although the coefficients of restitution are low (1-2%), these velocities are still above the negligible gravitational escape velocity of a 1 meter or even 10 meter planetesimal. At larger sizes, however, the weak gravity of the planetesimal may be

COLLIDE-2 results suggest that interparticle collisions in planetary rings may not enough to turn around impactors that rebound slowly off a regolith-covered surface. If be an important source for dust in the rings unless the ring is gravitationally perturbed so growth to these sizes involves collisions between aggregates, then the impactor might that impact speeds are several 10's of cm/s. Our results also suggest that collisional break into smaller particles which are subject to an aerodynamic growth mechanism accretion of planetesimals is problematic at large colllision velocities, and that either (Wurm et al., 2001) rather than rebounding as a single object.
gravitational instabilities or aerodynamic growth mechanisms are necessary, or that typical collision velocities are less than a few m/s until planetesimals are large enough for

References

Colwell, J. E., and M. Mellon 2002. Experimental Studies of Collisions in Planetary Rings and Protoplanetary Disks, 33rd Lunar and Planetary Science Conference, Mar. 11-15, Houston TX (Abs. #1757).

Colwell, J. E., L. W. Esposito, M. Horanyi 2002. Microgravity Impact Experiments: Results from COLLIDE-2. 6th Microgravity Fluid Physics and Transport Phenomena Conference, Aug. 14-16, Cleveland OH.

Wurm, G., J. Blum, and J. E. Colwell 2001. A new mechanism relevant to the formation of planetesimals in the solar nebula. *Icarus* **151,** 318-321.

ATTACHMENT

Low Velocity Impacts into Dust:

Results from the COLLIDE-2 Microgravity Experiment

Joshua E. Colwell
Laboratory for Atmospheric and Space Physics
University of Colorado, Campus Box 392
Boulder CO 80309-0392
(303) 492-6805
(303) 492-6946 (FAX)
josh.colwell@lasp.colorado.edu

November 14, 2002

Submitted to *Icarus*
Manuscript pages: 23
Figures: 9
Tables: 2

Suggested running head: Low Velocity Microgravity Impact Experiments

Address correspondance to:
Joshua Colwell
Laboratory for Atmospheric and Space Physics
University of Colorado
Campus Box 392
Boulder CO 80309-0392
Tel: 303-492-6805
Fax: 303-492-6946
josh.colwell@lasp.colorado.edu

We present the results of the second flight of the Collisions Into Dust Experiment (COLLIDE-2), a space shuttle payload that performs six impact experiments into simulated planetary regolith at speeds between 1 cm/s and 100 cm/s. COLLIDE-2 flew on the STS-108 mission in December 2001 following an initial flight in April 1998 (Colwell and Taylor, 1999). The experiment was modified since the first flight to provide higher quality data and the impact parameters were varied. Spherical quartz projectiles were launched into quartz sand and JSC-1 lunar regolith simulant. At impact speeds below ~20 cm/s the projectile embedded itself in the target material and did not rebound. Some ejecta was produced at lower speeds. At higher speeds the projectile rebounded and significant ejecta was produced. We present coefficients of restitution, ejecta velocities, and limits on ejecta masses. Ejecta velocities are typically less than 10% of the impact velocity, and the fraction of impact kinetic energy partitioned into ejecta kinetic energy is also less than 10%. Taken together with a proposed aerodynamic planetesimal growth mechanism (Wurm et al., 2001a), these results support planetesimal growth at impact speeds above the nominal observed threshhold of about 20 cm/s.

Key words: Planetary rings; planetesimals; experimental techniques; dust; collisions.

1. Introduction

Observations of dust in the ring systems of each of the giant planets suggest a continuing supply of dust liberated from the surfaces of larger "parent" ring particles (e.g. Cuzzi and Burns, 1988; Colwell and Esposito, 1990a; de Pater et al., 1999). Micrometeoroid bombardment of these parent objects provides one component of the dust source, but interparticle collisions may release a significant fraction as well (Colwell and Esposito 1990a, 1990b). Ring particles are likely coated with small particles reaccreted from the micrometeoroid ejecta (e.g. Cuzzi and Durisen 1990). Interparticle collision speeds in optically thick planetary rings have been collisionally damped, typically to speeds much less than 1 m/s. However, the small masses of ring particles makes gravity negligible in determining the fate of dust on the surfaces of these particles, even in very slow collisions. In addition to being a source of dust for dust rings, the coating of small particles on the surfaces of larger ring particles acts as an efficient shock absorber that damps random velocities excited, for example, by gravitational perturbations from nearby or embedded moons.

Similar types of collisions likely played an important role in the early stages of planetesimal growth. These collisions likely occurred at relative velocities from a few 10's of m/s for very different-sized particles down to 10's of cm/sec for a 1 cm object colliding with a 10 cm object, either a laminar or turbulent nebula (Weidenschilling and Cuzzi 1993). Velocities less than 1 m/s are significantly higher than escape velocities for centimeter-to-meter size particles, and so collisions must have been highly inelastic in order for growth to proceed. Dusty regoliths covering particles may have helped to

dissipate collisional energy, reducing the rate of mass loss during collisions and promoting accretional growth of larger bodies. However, if the particles consist of unconsolidated dust, then even at low velocities these aggregates may fragment and net erosion rather than accretion could occur. Blum and Wurm (2000), Wurm and Blum (1998), Blum et al. (2000), and Poppe et al. (2000) have experimentally studied the collisional growth of aggregates of dust. Wurm et al. (2001a, 2001b) have looked at the growth and erosion of dust aggregates in the presence of nebular gas drag on grains. The latter showed that even if small particles are liberated in a collision, they may quickly become entrained in the gas of the protoplanetary nebula and returned to the surface of the larger object and reaccrete. The amount of ejecta produced in such collisions, and the velocities of the resulting ejecta, are poorly understood.

The effects of surface properties, including frost and dust, on the coefficient of restitution in low velocity collisions have been experimentally studied by Bridges et al. (1984), Hatzes et al. (1988), Supulver et al. (1995), and Dilley and Crawford (1996) using hard ice particles and pendulums to achieve impact velocities less than 1 cm/s, typical of planetary ring particle impact velocities (e.g. Esposito, 1993). Hatzes et al. (1988) used frosted ice impactors such as might be found in planetary rings, but there was no unconsolidated regolith. Hartmann (1978) measured coefficient of restitution as a function of regolith thickness for normal impacts into granular material at 1 g acceleration. Hartmann (1985) performed impact experiments at speeds as low as 5.3 m/s into granular material and reported on the production of ejecta. Colwell and Taylor (1999; Paper 1 hereafter) reported on the first results from the microgravity experiment described here, which were the first to study ejecta production at speeds below 1 m/s. In

this paper we describe the results from the second flight of the Collisions Into Dust Experiment (COLLIDE-2) and its implications for the early stages of planetesimal formation and dust production in planetary rings.

In the next section we describe the experimental procedure, and in section III we present results from the flight data. We conclude with a discussion of the implications of the results on planetary ring and protoplanetary disk dynamics.

I. Experimental Procedure

In order to study low-velocity collisions into a dust-covered surface such as occur between small particles in space, a microgravity environment is necessary. COLLIDE first flew on the space shuttle as a Get Away Special (GAS) payload on STS-95 in April 1998 (Paper 1). The basic configuration of the experiment for the COLLIDE-2 flight is unchanged from that described in Paper 1. Here we summarize the experiment configuration and describe those changes to the experiment that were made to ensure proper functioning. A concurrent set of ground-based experiments has been performed for comparison with COLLIDE (Colwell and Mellon, 2002), and a series of reduced-gravity experiments on the NASA KC-135 reduced gravity aircraft is underway (Colwell et al., 2002).

COLLIDE-2 is a self-contained autonomous payload that was part of the MACH-1 Hitchhiker bridge on space shuttle Endeavour mission STS-108. The experiment performs six independent impacts at normal incidence angle into a bed of granular material. Each impact takes place in a self-contained and independent Impactor Box System (IBS). The impacts are recorded on two digital video tapes recorded by digital video camcorders inside the experiment. The experiment container was evacuated and sealed prior to launch. The camcorders are in two sealed containers at 1 atmosphere of pressure to provide a normal operating environment. A baroswitch on the exterior of the container turned on the experiment electronics within the first minute of the launch. The experiment program follows a 14-hour software timer before beginning execution of the experiment during a crew sleep period to minimize accelerations. Two data loggers were flown to provide verification of experiment operation and timing. A temperature data logger with four temperature sensors recorded increases in temperatures as voltage regulators turned on during execution of the experiment. A light-sensitive data logger was positioned to detect the lights inside IBS 3. This provided another indication of the timing of the experiment for correlation with telemetry on the space shuttle attitude control system which automatically fires thrusters on the orbiter to maintain attitude. The orbiter launched at 22:19 UTC on December 5, 2001. The first experiment activity was a three-minute warm-up of each of the camcorders. This is a change from the first flight of COLLIDE to counter camera recording problems the first time the cameras

were used. The sealed containers for the cameras were redesigned to prevent a recurrence of the leaks on the first flight. One camera container experienced partial leaking on COLLIDE-2, however both cameras functioned properly. The ambient pressure in the experiment canister was less than 10 torr.

Temperature increases were observed in the data logger records from the temperature sensors mounted near the voltage regulators controlling the cameras. The temperature data indicate an experiment start time of 12:21:00 UTC on December 6, 2001. The timing of each impact experiment is controlled by the experiment software and is determined from the experiment start time. The final impact experiment was finished at 12:50:00 UTC. Comparison of the experiment impact times with data from the space shuttle orbiter's Reaction Control System firing times showed that no thruster firings occurred during the impacts. Video data also show no indications of any residual accelerations. Data were returned on the two digital videotapes and retrieved for analysis from the experiment in January 2002.

Two different target materials were used on COLLIDE-2: silica (quartz) sand and JSC-1 lunar regolith simulant. Both samples were seived to a size distribution between 75 and 246 _m. The silica particles are rounded in shape while the JSC-1 particles are angular (Figure 1). Average grain size for the silica particles is 220 _m, while the average size for unsieved JSC-1 is about 100 _m. JSC-1 is a glass-rich basaltic ash which has similar chemical composition, mineralogy, particle size distribution, and engineering properties to lunar mare regolith (McKay et al. 1994). The internal angle of friction of JSC-1 is 45 degrees, while for the silica sand it is 34 degrees. Although both of these numbers depend on the confining pressure, the difference reflects the rounder shape of the sand particles making them less able to sustain a steep slope. For the impact experiments described here, this means that the particles in the sand targets are more free to roll across each other in response to an impact while JSC-1 particles behave more like interlocking gears.

Minimal filling of the target trays under 1 Earth gravity corresponds to a relative density, $D_r = 0$, where relative density is defined by

$$D_r = \frac{e_{max} - e}{e_{max} - e_{min}}. \quad (1)$$

A relative density of 1 corresponds to the density of the material achieved following vibration with a compressive force on the material. The material constants e_{max} and e_{min} are determined experimentally by measuring void ratios of the material following compression and vibration (e_{min}) and with no load applied (e_{max}). The void ratio, e, is the volume of voids divided by the volume of solids,

$$e = \frac{G_s \rho_w}{\rho_d} - 1 \quad (2)$$

where G_s is the specific gravity of the material, ρ_w is the density of water, and ρ_d is the bulk density of the sample. The void ratio is related to the porosity, n, by n=e/(1+e). For

JSC-1, G_s=2.9, e_{max}=1.028, and e_{min} =0.585. For the silica particles, G_s =2.65, e_{max}=0.805, and e_{min} =0.486. On COLLIDE-2 each IBS was filled as closely as possible to a relative density of 0, by not using any shaking or compression of the samples, and not overfilling the target tray volumes. The main uncertainty in this value is in the actual free volume available to the target material because of the presence of flexible materials within the target tray designed to prevent jamming of the target tray door mechanism. Because all the samples are subjected to two minutes of extreme vibration during launch of the shuttle there is the possibility of settling and an increase of the relative density. We tested the response of our samples to vibration on the ground and found that there was no significant compression of the quartz sand due to vibration alone, and removing the particles small than 75 _m significantly reduced the settling of the JSC-1 seen in the first flight of COLLIDE.

Another possible consequence of the launch vibration is leaking of the target grains into the door mechanism. Two of the six IBS target tray doors jammed on the first flight (paper 1), so a new system of particle barriers was designed for COLLIDE-2. This involved a vacuum grease seal along the inside boundary of the target tray door which reduced the volume of the trays by about 1 cm^3 compared to a total volume of 229 cm^3. The uncertainty in the target mass is less than 1 gm out of approximately 300 gm, so the uncertainty in the bulk density is less than 1 per cent. Each target tray door functioned properly on COLLIDE-2. The bulk densities, void ratios, and porosities for each IBS are included in Table 1 along with measured impact parameters. For comparison, the porosity of the top 1 cm of lunar regolith is 0.59, corresponding to a bulk density of 1.4 g/cm^3 , based on interpretation of microwave observations during a lunar eclipse (Sandor and Clancy 1995).

Table 3: Experimental Parameters

IBS Parameter	1	2	3	4	5	6
Measured Impact Speed (cm/s)	110±10	3.60±0.1	1.29±0.01	81±10	12.2±0.1	28±2
Projectile mass (g)	10.71	9.64	10.29	8.66	8.98	10.62
Target material	Quartz Sand	Quartz Sand	Quartz Sand	Quartz Sand	JSC-1	Quartz Sand
Target bulk density (g/cm^3)	1.49	1.53	1.50	1.52	1.25	1.49
Target void ratio	0.78	0.73	0.77	0.74	1.32	0.78
Target porosity	0.44	0.42	0.43	0.43	0.57	0.44
Target Relative Density	0.07	0.23	0.12	0.18	N/M	0.09

The density of the projectiles is 2.65 g/cm^3. Both target materials were sieved to particle size ranges of 75-250 microns. The void ratio for the JSC-1 target exceeds the nominal maximum value for JSC-1 because all particles smaller than 75 microns were removed. These small particles would normally fill void spaces leading to a lower porosity. For this reason the relative density of the JSC-1 target is not measured (N/M). Uncertainties in impact speed are based on uncertainty in measuring impactor position. This is controlled by pixel size at the slowest speeds and image smear at the fastest speeds.

The geometry of the impacts, the camera views, and the sequence of operation of the experiment are the same as described in paper 1. The only change to the experiment sequence was the addition of camera warm-up periods prior to running the experiment. The experiment was powered by its internal set of 24 D-cell alkaline batteries in three redundant parallel stacks of 8 cells.

I. Experimental Results

A. Overview

Except for the data logger temperature and light sensor engineering data mentioned above, all COLLIDE-2 data are contained on two digital videotapes recorded by the onboard camcorders. Because each camcorder has a fixed orientation and views three IBSs at the opposite end of the experiment simultaneously, each IBS only fills about one-sixth of the camcorder field of view. The data are therefore at low spatial resolution, and the target silica and JSC-1 grains are sub-pixel. An example frame from

IBS 1 is shown in Figure 2 with a schematic identifying elements in the scene. The objectives for COLLIDE-2 were (i) to identify the transition between impacts that produce significant ejecta (erosional impacts) and those that do not produce ejecta (accretional impacts), (ii) to measure coefficients of restitution for impacts into regolith at low impact velocities, (iii) to measure the velocity of ejecta produced in the impact, and (iv) to constrain the ejecta mass. The range of impact velocities was chosen to span the likely transition regime based on results from COLLIDE and ground-based impact experiments at 1 m/s and higher speeds.

All six IBSs operated nominally, and Table 2 summarizes the outcomes of each impact experiment. The experiment successfully met the primary objective of bracketing the transition between erosional and accretional impacts which, for the materials and impactor sizes studied here, occurs at an impact speed of about 10-20 cm/s. We were also able to measure normal coefficients of restitution, $\varepsilon_n = v_n/v_i$, where v_n is the normal component of the rebound velocity, v_i is the impact velocity. Tangential coefficients of restitution were not measured, however, because in those impacts where the projectile rebounded, fiduciary marks on the projectiles were not visible for tracking rotation due to interference from ejecta particles. In two of the six impact experiments no ejecta was produced. In three of the remaining four the ejecta curtain was optically thick and because the particles are sub-pixel scale, only a gross characterization of ejecta velocities was possible. In the final impact, individual ejecta particles were tracked providing a

direct measure of ejecta velocities. The details of the ejecta velocity analysis are below. Ejecta masses cannot be measured directly because some target particles are released from the target after the impact by the closing of the target tray door. In addition, static charging of the target surface prior to the impact by the opening of the target tray door resulted in some particles leaving the surface prior to the impact. An upper limit on ejecta mass can be placed from the amount of target material recovered from the target tray, but more meaningful estimates are arrived at from comparison of the video data with video data from ground-based experiments with measured ejecta masses.

Projectile velocities before and after impact were obtained by measuring the change in position of the projectile from one frame to the next of the digital videotape. The frame rate is 29.97 frames per second, so the uncertainty in speeds is larger at higher speeds. Tracking data indicating the trajectory for the projectile from IBS 1 after impact are shown in Figure 3. The change in direction is the result of a collision with the side wall of the IBS. The scatter in points is primarily a result of the projectile moving less than one pixel per frame. Projectile trajectories were tracked manually using Spotlight tracking software provided by NASA Glenn Research Center. Velocities are measured from tracking data like that shown in Figure 4 for the projectile in IBS 2 prior to impact.

Table 4: Experiment Summary

IBS	Impact Speed (cm/s)		Rebound Speed (cm/s)		ε_n	Crater Diameter (cm)	Maximum Ejecta Velocity (cm/s)
	X	Y	X	Y			
1	110±10	0±2	1.10	0.85	0.01	6±2	10±1
2	0.01±0.01	3.62±0.04	0	0	0	0	0
3	1.29±0.01	0.14±0.04	0	0	0	0	0
4	81±10	0±2	1.2	0.67	0.015	N/M	16±1
5	0.12±0.06	12.15±0.1	0	0	0	0	1.5±0.2
6	24.9±2	2.4±1	0.50	0.32	0.02	4±2	3±1

Notes: Speed uncertainties are the higher of the formal 1-sigma uncertainty in the fit to the trajectory data or the uncertainty introduced by smear in the image. ε_n is the ratio of the normal component of the rebound velocity to the normal component of the impact velocity. Movement out of the X-Y plane was not measured. N/M = Not measured. Crater diameters of 0 represent impacts where the impactor embedded itself in the target without creating a detectable larger displacement of target material. See text for details on ejecta velocities.

B. Coefficient of Restitution.

Bridges et al. (1984) and Hatzes et al. (1988) performed impact experiments with frosted and unfrosted ice spheres at velocities less than 1 cm/s and found a relationship between coefficient of restitution and impact speed. Dilley (1993) examined the functional dependence of the coefficient of restitution on particle size and mass, and Dilley and Crawford (1996) performed ice impact experiments at 1 cm/s with different impactor masses. Supulver et al. (1995) performed [illegible] collisions of ice [illegible]

C. Ejecta Velocities.

The impact of IBS-5 at 12 cm/s produced a sparse ejecta curtain of particles that could be individually tracked. These particles were tracked in the same way that the projectiles were tracked for impact and rebound velocities, though some ejecta particles were tracked using automatic tracking features of the Spotlight tracking software. Because the particles are sub-pixel, their brightness varies, and they are occasionally lost from view when passing in front of light markings on the background.

Particles were therefore only tracked over parts of their trajectories, and manual tracking was used when the automatic tracking could not lock onto particles consistently. Figure 5 shows the trajectories of 26 particles from the impact in IBS 5. We estimate that this represents approximately one half of all the ejecta particles and clumps released in the impact. Full sampling of ejecta trajectories was not possible because some particles are too faint to be reliably tracked against the background, either because of small size, a path that lay consistently in front of one of the bright background markings, or a path in front of or behind the projectile. 37 particles were tracked and later analysis showed that only 26 of these were unique. The last 8 particles selected for tracking were duplicates of previous particles, so we believe all particles that could be reliably tracked have been tracked.

Figure 6 shows the X and Y components of the measured ejecta speeds, V_X and V_Y. The component of the velocity out of the camera plane was not measured. The relative lack of particles with small V_Y is a selection effect: the impact was in the Y direction, and particles with small V_Y were too close to the target surface, where the background was bright and cluttered by loose particles, for tracking. 24 of the 26 particles had $V_X<V_Y$, consistent with a simple ejecta cone model with a cone opening angle of 45 degrees or less, where smaller V_X corresponds to larger V_Z, which could not be measured. The distribution of ejecta velocities measured from the X and Y components is shown in Figure 7; in the simple ejecta cone model the total ejecta velocity is simply $V_Y/\cos\_$.

Making this assumption results in an ejecta velocity distribution similar to that for the X and Y components alone: most particles' velocities are between 0.3 and 0.8 cm/s.

In the three remaining experiments in which ejecta was produced on impact, we have measured the velocities of the ejecta curtains but not individual particles. The schematic in Figure 2 shows five components of the ejecta curtain for IBS 1. For this impact at 110 cm/s, the ejecta boundary velocities indicate a maximum ejecta velocity of ~10±1 cm/s, and the velocities of each measured boundary are given in Figure 2. The speed of the center of the ejecta curtain (V_A = 7.2±0.2 cm/s) is the projected speed in the image plane, while the speeds along the diagonal tracks (V_B and V_C) have no projection effect. A cone opening angle of 45 degrees corresponds to a full speed at the center of the ejecta curtain of $V=V_A/\cos(\pi/4)=10.2$ cm/s, compared with the values for V_B and V_C of 8.7 and 11.1 cm/s, respectively.

The impact in IBS 4 at 81 cm/s resulted in slightly higher maximum ejecta velocities of 16 cm/s. That impact produced discrete rays of ejecta in the curtain. The trajectories of tracked points on the ejecta curtain along with the velocities (in the plane of the image) are shown in Figure 8. The target in IBS 4 was slightly more dense than the target in IBS 1, but there is insufficient data to conclusively link that to the higher ejecta speeds. The impact in IBS 6 at 25 cm/s produced a cloud of ejecta that was too dense for individual particle tracking but not as symmetric or with as clearly identifiable ejecta curtain boundaries as in IBS 1 and IBS 4. The projectile struck the surface at a slightly

oblique angle (Table 2) resulting in an asymmetric distribution of ejecta (Figure 9). We tracked seven points along the ejecta boundary using both manual and automatic tracking resulting in ejecta velocities of 1.5 to 3.5 cm/s. Roughly, the results from the four impacts that produced measurable ejecta indicate a maximum ejecta speed of 10-15% of the impactor speed.

D. Ejecta Mass

Direct measurement of the ejecta mass could only be achieved by comparing the target mass in the target tray before and after the flight. Some particles were lifted off the target surface prior to impact by electrostatic forces, and the target.tray doors did not completely reseal the target tray after impact. Therefore the measured amount of remaining target material only provides a rough upper limit on the ejecta mass. Comparisons with the video data show that even in the case where clearly no impact ejecta was produced the amount of material that left the target tray due to these two effects was over 40 gm. For comparison, assuming that all the kinetic energy of the impactor went into kinetic energy of the ejecta provides upper limits on the ejecta mass between 110 and 530 gm which are clearly far higher than the actual ejecta masses. For the two fastest impacts the results indicate that at most 15% of the available kinetic energy was partitioned into ejecta kinetic energy. Given that we observe a significant loss of target material prior to the impact and that not all of the ejecta are moving at the maximum speeds, the actual ejecta kinetic energy fraction is lower by at least a factor of 2.

While the JSC-1 target had a significantly higher porosity than the quartz sand targets, the more angular nature of the grains may have reduced the amount of flow in the target in response to the impact and therefore reduced the amount of ejecta liberated from the surface. Ground-based experiments at 1-2.3 m/s have shown that the size distribution and angularity of the target grains plays an important role in the amount of ejecta produced (Colwell and Mellon 2002).

II. Conclusions and Discussion

The impact experiments described here are in the same velocity and gravity regime as many impacts in planetary rings and protoplanetary disk environments. However, they cannot be considered as direct simulations of those collisions because we use different materials and we do not collide two dust-coated, free-floating, irregular, simulated ring particles. However, with the results from two flights of COLLIDE and our ongoing ground-based and airplane-based experiments, we can begin to draw some general conclusions about the behavior of small particles in microgravity collisions and

Colwell and Esposito (1990a, 1990b) modeled the production of dust in the ring systems of Uranus and Neptune from a combination of micrometeoroid bombardment of macroscopic ring particles and moonlets and collisions between ring particles. For dust production from ring particles their nominal model produced roughly two thirds of the observed dust from interparticle collisions and one third from micrometeoroid ejecta (Colwell and Esposito, 1990a (CE90), their Table II). In the absence of appropriate experimental data they used the same model for ejecta mass for high velocity and low velocity collisions. This model predicts 10^{-3} gm of ejecta for impacts like those in IBSs 1 and 4 on COLLIDE-2, and less for the lower velocity impacts but with no lower cutoff. The collisions in COLLIDE-2 produced far more ejecta at 100 cm/s than the CE90 model predicts, however that model also predicts significant ejecta at 10 cm/s if the masses of

Experimental studies of the collisional accretion in the early stages of
the colliding objects are large. The COLLIDE-2 data reported here only show a variation planetesimal growth have shown that micron-sized grains can stick at impact speeds
in impact speed, so further experiments are needed to learn the effects of impactor size below about 1.1 m/s (Poppe et al., 2000), and that entrainment of rebounding dust can and mass. Extrapolating the COLLIDE-2 results to the Uranus moonlet belt size regime result in net growth at collision speeds as much as 10 times higher than that (Wurm et al., suggests that collision velocities are slightly higher than the 10 cm/s used by CE90, or 2001b). Our experiments use significantly larger particles (mean particle size of 150_m that most of the dust is generated by micrometeroid impacts rather than interparticle compared to 1_m for the aggregation experiments), and consequently surface forces such collisions. The latter can be accomplished by making the size distribution of the moonlets as the van der Waals force are less effective. Particle sticking from electrostatic dipole steeper or the optical depth higher so that more surface area is exposed to the charge distribution (Marshall 1998) may be important in suppressing ejecta at the lower micrometeroids. The observational constraints are not strong enough to rule out either impact speeds. We observe a threshhold velocity of about 20 cm/s between erosive and hypothesis, and the extrapolation of COLLIDE-2 results to much larger impactors must sticking impacts (significant ejecta and impactor rebound at 25 cm/s, and little ejecta with be considered speculative until more data are collected.
no rebound at 12 cm/s). This is far lower than what might be inferred from the amount of ejecta produced in ground-based impact experiments (e.g. Hartmann 1985, Weidenschilling and Davis, 1988) which suggest a threshhold of about 10 m/s. The ejecta

velocities are low enough, however, that the aerodynamic growth mechanism of Wurm et al. (2001b) could make even the 1 m/s impacts in COLLIDE-2 lead to growth rather than erosion. In this model, small particles liberated in an impact are returned to the target surface after becoming entrained in the nebular gas. This mechanism works as long as the ejecta are small enough to allow rapid coupling to the gas and the growing planetesimal is large enough to be decoupled from it. This threshhold must also depend on other parameters not varied in the COLLIDE-2 experiment, such as impactor strength, target size, and impactor size. Further experiments are planned and underway to investigate the effects of varying these parameters (e.g. Colwell and Mellon 2002, Colwell et al. 2002).

We found that our 2-cm impactors rebounded at 28 cm/s and stuck at 12 cm/s, while on the first flight of COLLIDE impactors at 17 cm/s into denser targets also rebounded. Although the coefficients of restitution are low (1-2%), these velocities are still above the negligible gravitational escape velocity of a 1 meter or even 10 meter planetesimal. At larger sizes, however, the weak gravity of the planetesimal may be enough to turn around impactors that rebound slowly off a regolith-covered surface. If growth to these sizes involves collisions between aggregates, then the impactor might break into smaller particles which are subject to the aerodynamic growth mechanism rather than rebounding as a single object. We plan further experiments to study impacts of dust aggregates into regolith which would help answer this question. If, on the other hand, the small particles have formed bonds through sintering that are too strong to break in these slow collisions, then we have a 20 cm/s maximum impact velocity for planetesimal growth to occur in the meter size range. At 1 AU, this random velocity corresponds to a disk scale height of only $\sim 10^3$ km.

Acknowledgments: This research was supported by NASA. Technical support from NASA's Shuttle Small Payloads Program office, Glenn Research Center, Brian Motil, Monica Hoffmann, and the Kennedy Space Center is gratefully acknowledged. This paper benefitted from discussions with Larry Esposito, Mihály Horányi, Glen Stewart, Stein Sture, and Gerhard Wurm.

REFERENCES

Barge, P. and R. Pellat 1991. Mass spectrum and velocity dispersions during planetesimal accumulation. *Icarus* **93**, 270-287.

Blum, J., and 26 colleagues 2000. Growth and form of planetary seedlings: Results from a microgravity aggregation experiment. *Phys. Rev. Lett.* **85**, 2426-2429.

Blum, J., and G. Wurm 2000. Experiments on sticking, restructuring, and fragmentation of preplanetary dust aggregates. *Icarus* **143,** 138-146.

Bridges, F. G, A. P. Hatzes, and D. N. C. Lin 1984. Structure, stability, and evolution of Saturn's rings. *Nature* **309**, 333-335.

Colwell, J. E., and L. W. Esposito 1990a. A numerical model of the Uranian dust rings. *Icarus* **86**, 530-560.

Colwell, J. E., and L. W. Esposito 1990b. A model of dust production in the Neptune ring system. *Geophys. Res. Lett.* **17**, 1741-1744.

Colwell, J. E., and M. Taylor 1999. Low Velocity Microgravity Impact Experiments into Simulated Regolith. *Icarus* **138**, 241-249.

Colwell, J. E., and M. Mellon 2002. Experimental Studies of Collisions in Planetary Rings and Protoplanetary Disks, 33rd Lunar and Planetary Science Conference, Mar. 11-15, Houston TX (Abs. #1757).

Colwell, J. E., S. Sture, A. Lemos 2002. Microgravity Impact Experiments: The PRIME Campaign on the NASA KC-135. 6th Microgravity Fluid Physics and Transport Phenomena Conference, Aug. 14-16, Cleveland OH.

Cuzzi, J. N., and J. A. Burns 1988. Charged particle depletion surrounding Saturn's F ring: Evidence for a moonlet belt? *Icarus* **74**, 284-324.

Cuzzi, J. N., and R. H. Durisen 1990. Bombardment of planetary rings by meteoroids: General formulation and effects of oort cloud projectiles. *Icarus* **84,** 447-466.

De Pater, I., M. R. Showalter, J. A. Burns, P. D. Nicholson, M. C. Liu, D. P. Hamilton, and J. R. Graham 1999. Keck Infrared Observations of Jupiter's Ring System near Earth's 1997 Ring Plane Crossing. *Icarus* **138**, 214-223.

Dilley, J. P. 1993. Energy loss in collisions of icy spheres: Loss mechanism and size-mass dependence. *Icarus* **105**, 225-234.

Dilley, J. P., and D. Crawford 1996. Mass dependence of energy loss in collisions of icy spheres: An experimental study. *J. Geophys. Res.* **101**, 9267-9270.

Esposito, L. W. 1993. Understanding Planetary Rings. *Annu. Rev. Earth Planet. Sci.* **21**, 487-523.

Hartmann, W. K. 1978. Planet formation: Mechanism of early growth. *Icarus* **33**, 50-62.

Hartmann, W. K. 1985. Impact experiments. 1. Ejecta velocity distributions and related results from regolith targets. *Icarus* **63**, 69-98.

Hatzes, A. P., F. G. Bridges, and D. N. C. Lin 1988. Collisional properties of ice spheres at low impact velocities. *Mon. Not. R. Astr. Soc.* **231**, 1091-1115.

Marshall, J. R. 1998. "Coulombic Viscosity" in granular materials: Planetary and astrophysical implications. 29th Lunar and Planetary Science Conference, Houston TX.

McKay, D. S., J. L. Carter, W. W. Boles, C. C. Allen, and J.H. Allton 1994. JSC-1: A new lunar soil simulant. *In Engineering, Construction, and Operations in Space IV*, American Society of Civil Engineers, 857-866.

Poppe, T., J. Blum, and T. Henning 2000. Analogous experiments on the stickiness of micron-sized preplanetary dust. *Astrophys. J.* **553,** 454-471.

Sandor, B. J., and R. T. Clancy 1995. Microwave observations and modeling of a lunar eclipse. *Icarus* **115**, 387-398.

Supulver, K. D., F. G. Bridges, and D. N. C. Lin 1995. The coefficient of restitution of ice particles in glancing collisions: Experimental results for unfrosted surfaces. *Icarus* **113**, 188-199.

Weidenschilling, S. J., and D. R. Davis 1988. Dust to dust: Low-Velocity impacts of fragile projectiles. 19th Lunar and Planetary Science Conference, Houston TX.

Weidenschilling, S. J., and J. N. Cuzzi 1993. Formation of planetesimals in the solar nebula. In Protostars and Planets III (E. H. Levy, J. I. Lunine, Eds.), pp. 1031-1060, Univ. Arizona Press, Tucson.

Wurm, G., and J. Blum 1998. Experiments on preplanetary dust aggregation. *Icarus* **132**, 125-136.

Wurm, G., J. Blum, and J. E. Colwell 2001a. A new mechanism relevant to the formation of planetesimals in the solar nebula. *Icarus* **151,** 318-321.

Wurm, G., J. Blum, and J. E. Colwell 2001b. Aerodynamical Sticking of Dust Aggregates. *Phys. Rev. E*, **64**, #046301.

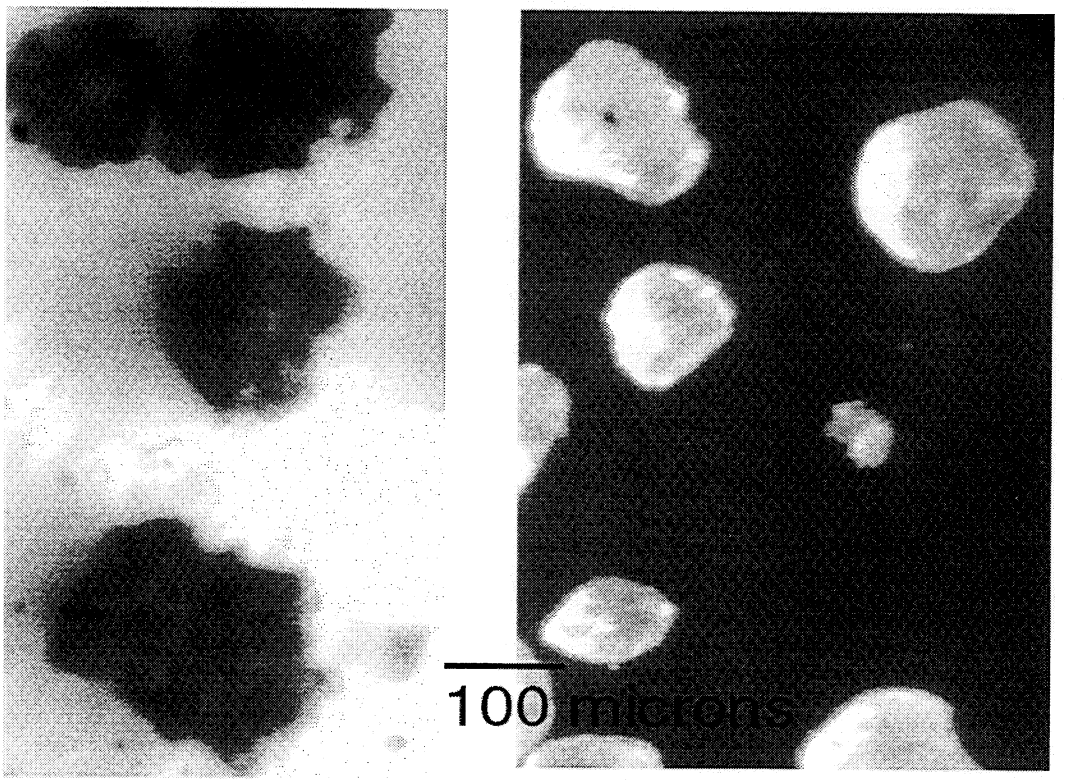

Figure 1: Photographs of JSC-1 particles (left) and silica quartz sand (right) used as target materials in COLLIDE-2. The scale bar is 100 microns long.

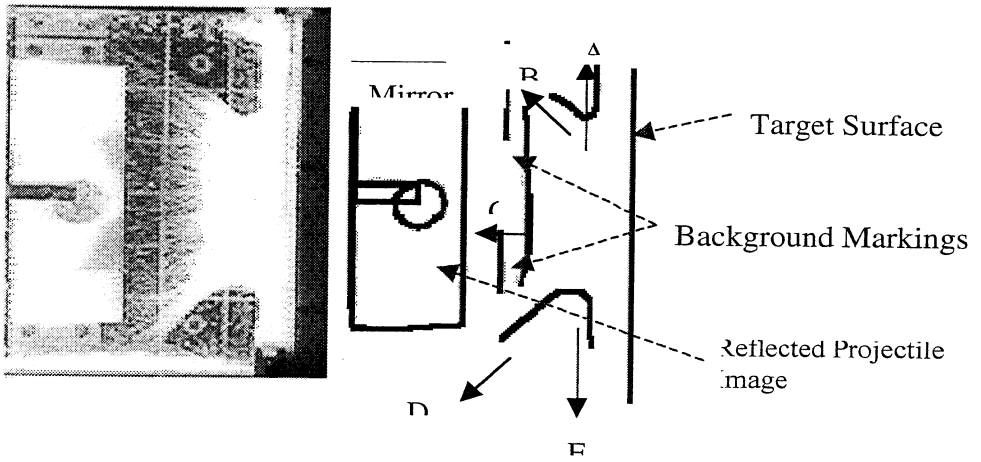

Figure 2: Still frame from IBS 1 0.3 seconds after impact and schematic of the image frame. The target surface is vertical at right, and the projectile motion was horizontally from the left. An image of the projectile on the target surface is visible in the mirror at left. Lettered arrows indicate the points on the ejecta curtain that were tracked for this IBS. Similar points on the ejecta curtains of IBS 4 and IBS 6 were tracked. Measured velocities of each point: $V_A = 7.2 \pm 0.2$ cm/s; $V_B = 8.7 \pm 0.3$ cm/s; $V_C = 11.1 \pm 0.4$ cm/s; $V_D = 1.7 \pm 0.1$ cm/s; $V_E = 2.7 \pm 0.1$ cm/s.

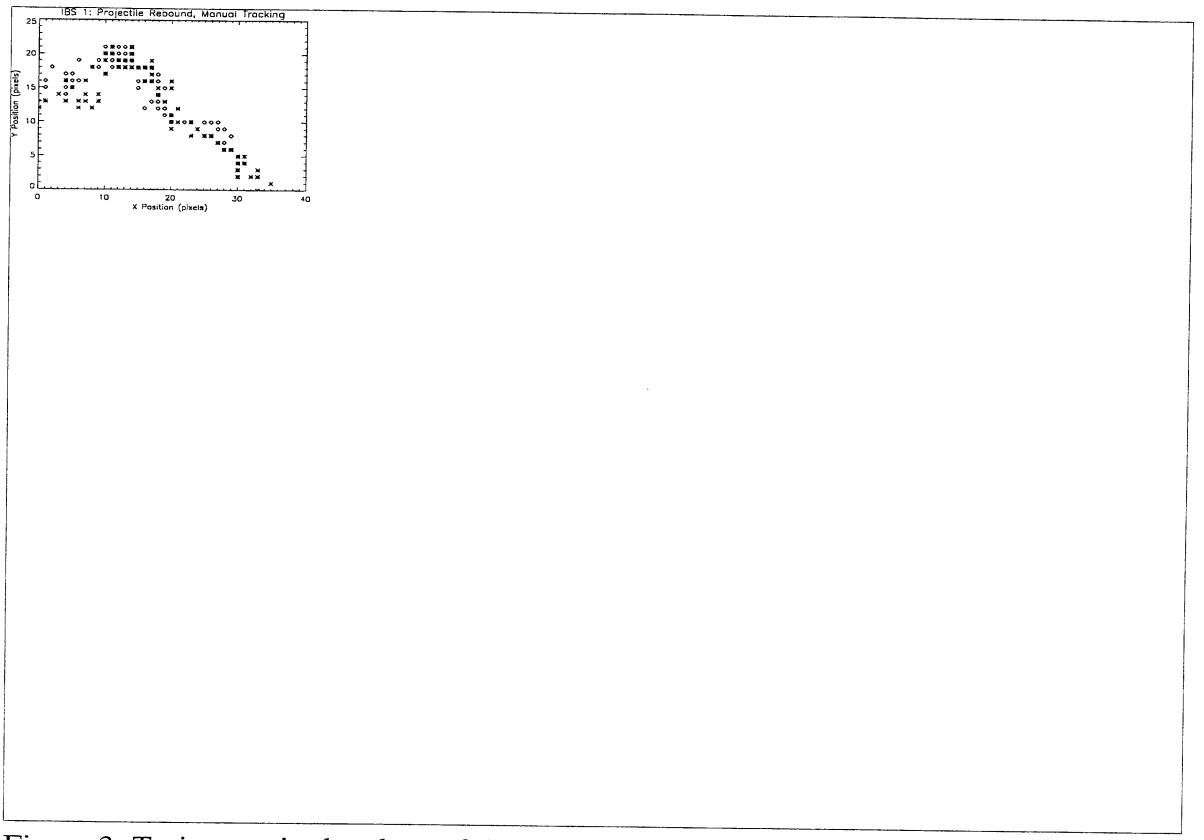

Figure 3: Trajectory in the plane of the video data of the projectile in IBS 1 after impact onto the target surface. Projectile positions were manually tracked twice and both sets of tracking data are shown (diamonds and asterisks). Time moves from right to left on this trajectory, and the change in direction at X=12 is due to the projectile bouncing off the IBS wall. The data at X>12 were used to determine the rebound speed from the target surface. The scale is about 13 pixels/cm in the X direction and 14 pixels/cm in the Y direction.

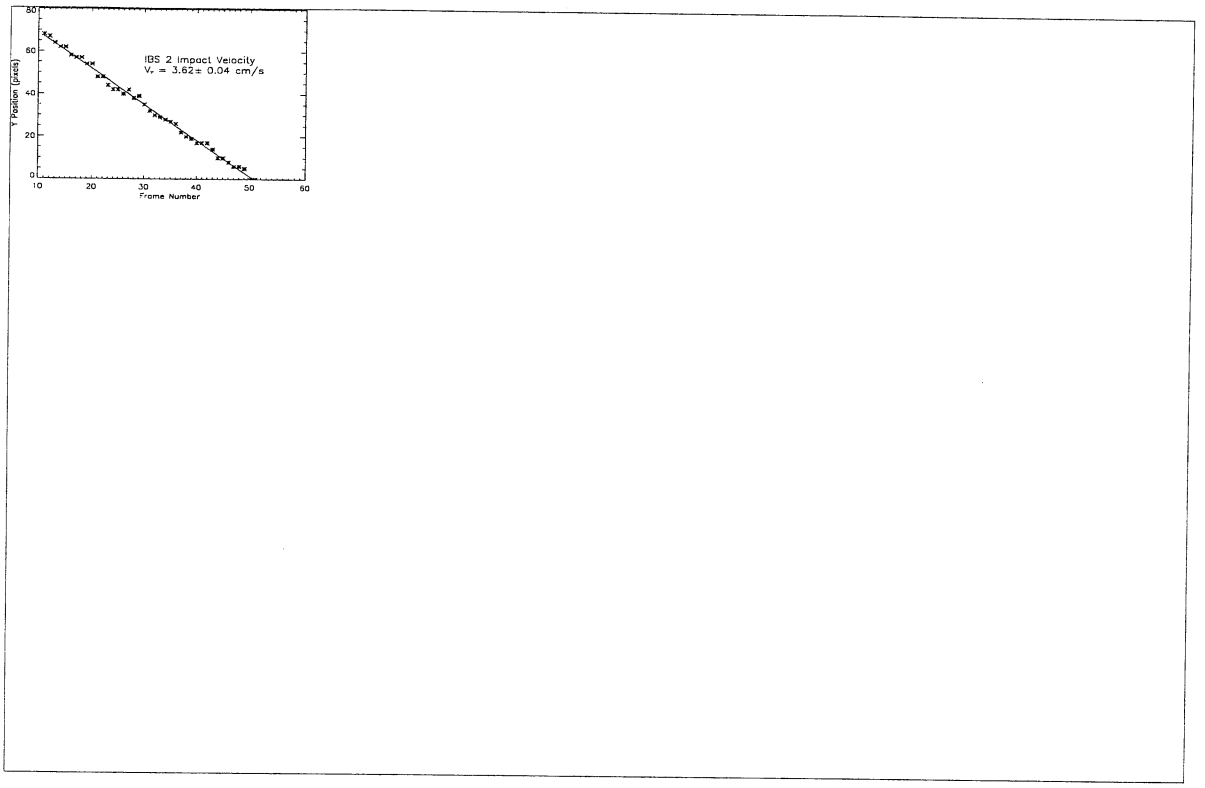

Figure 4: Position as a function of time for the projectile in IBS 2, with the best linear fit and derived impact speed. Individual projectile positions were manually selected.

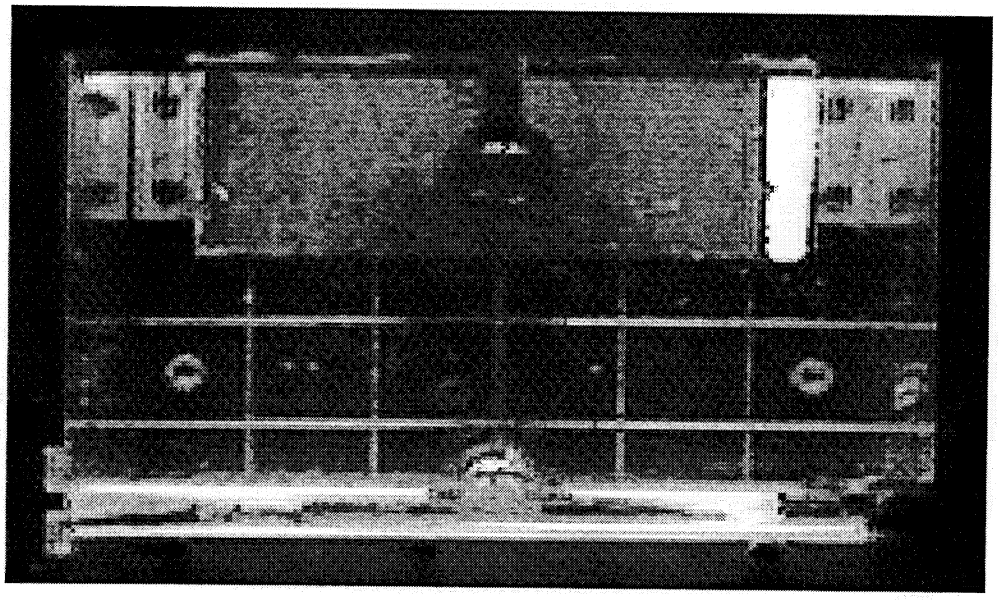

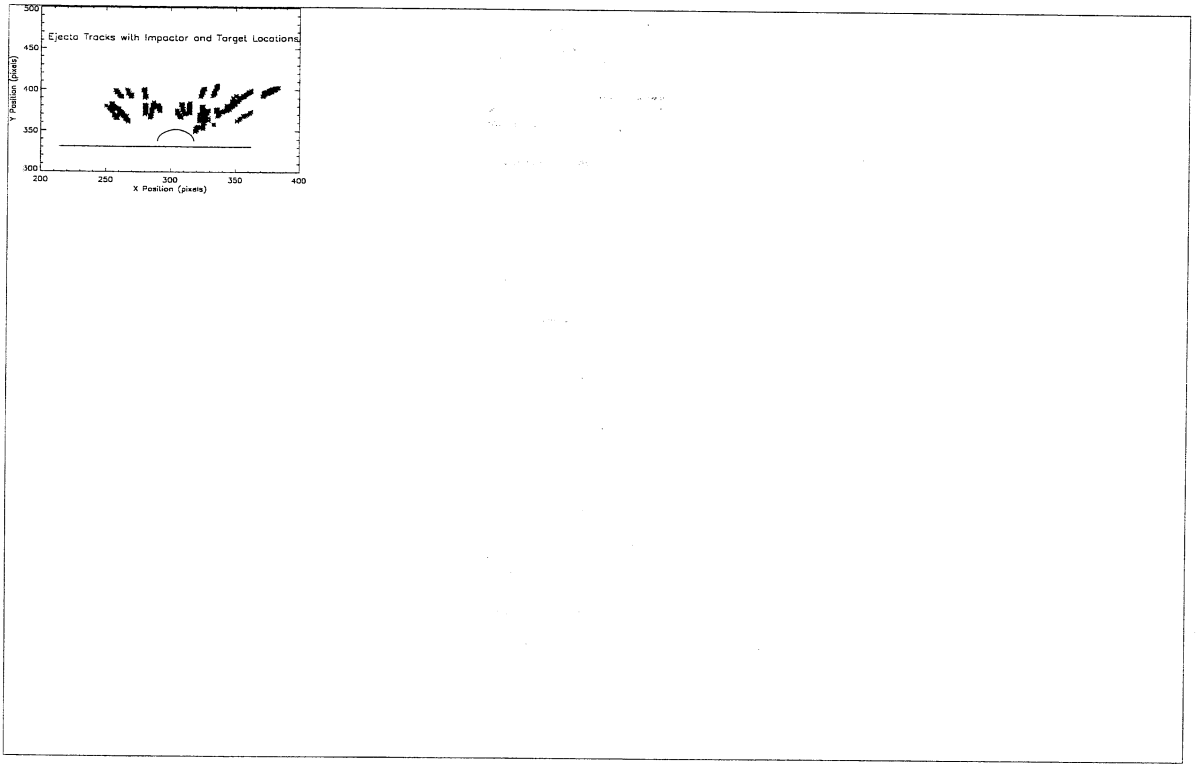

Figure 5: A frame from the impact in IBS 5 (top) showing individual clumps of ejecta (bright spots against the grid background). The bottom frame shows a superposition of

the trajectories of individual particles and clumps of particles ejected in the impact in IBS 5, with the target surface and post-impact projectile position indicated.

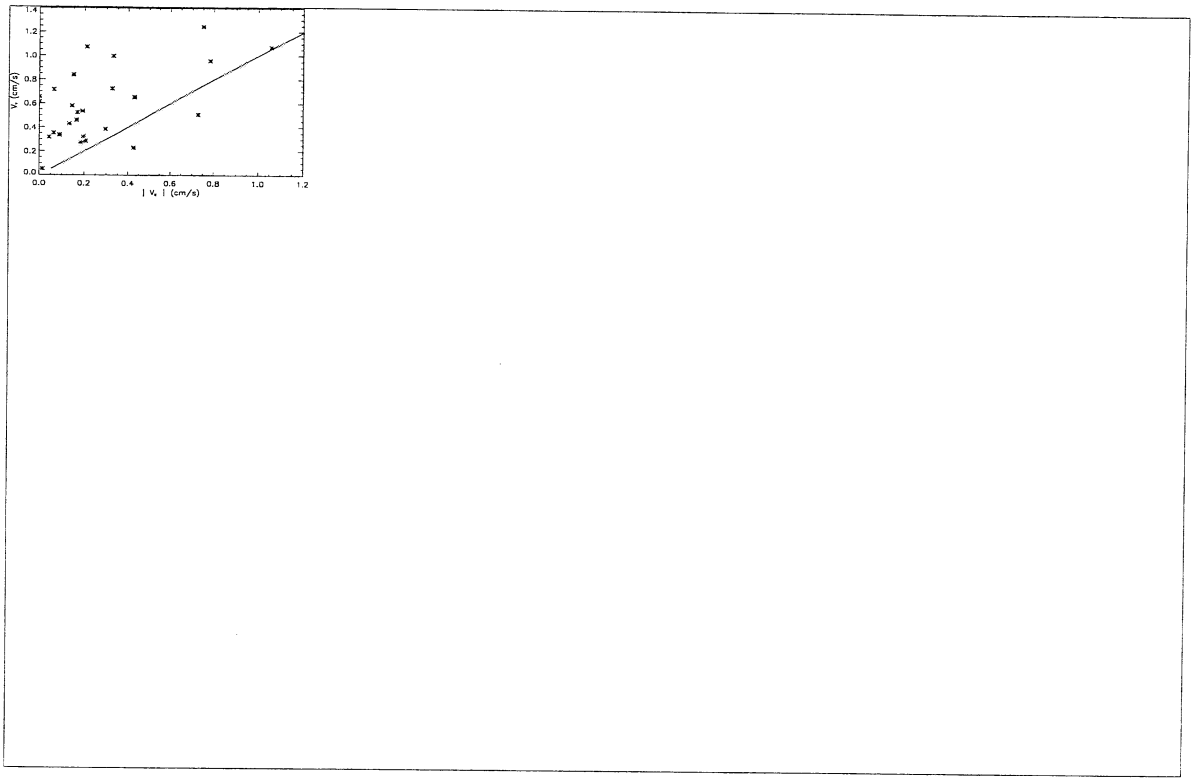

Figure 6: Scatter plot of measured V_X and V_Y components of ejecta from the IBS 5 impact. Only the two particles below the line had $V_X > V_Y$. The rest are consistent with an ejecta cone opening angle of 45 degrees (or less, measured from the surface normal).

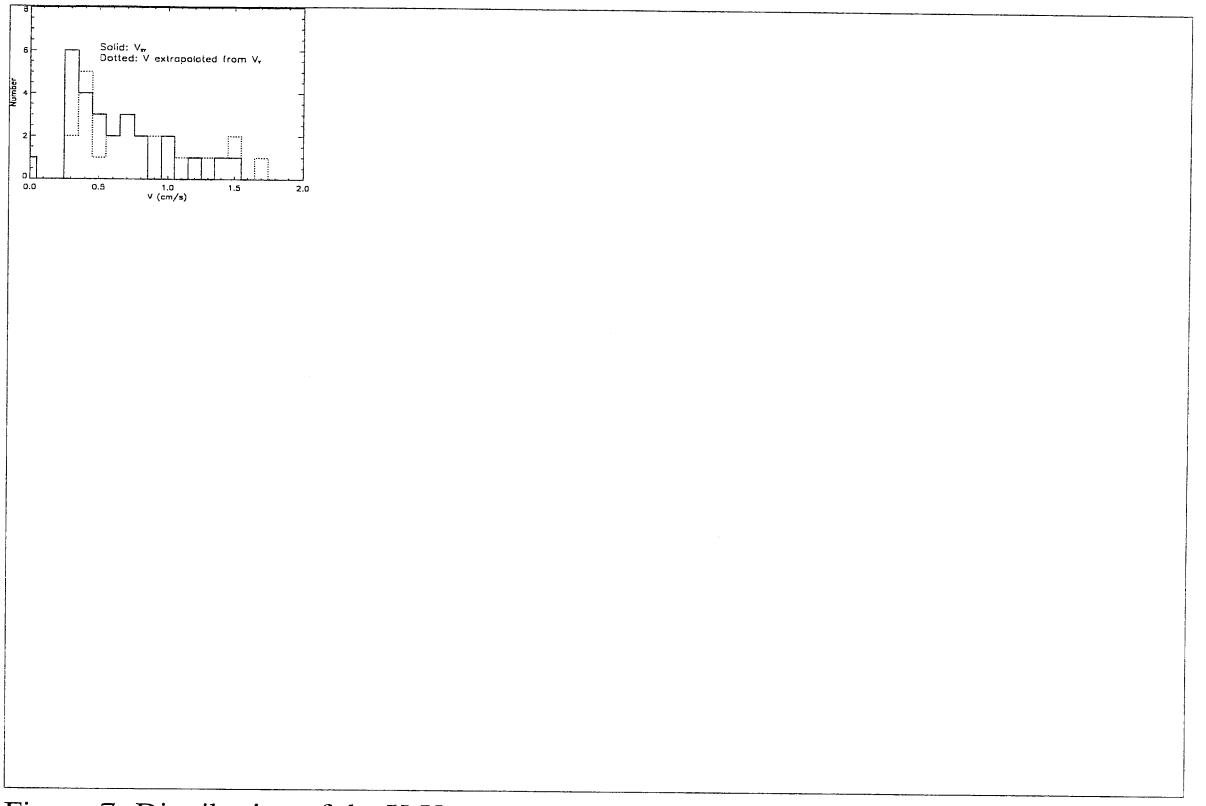

Figure 7: Distribution of the X-Y components of the ejecta in IBS 5 (solid), and distribution of velocities assuming that the ejecta launch angle is 45 degrees.

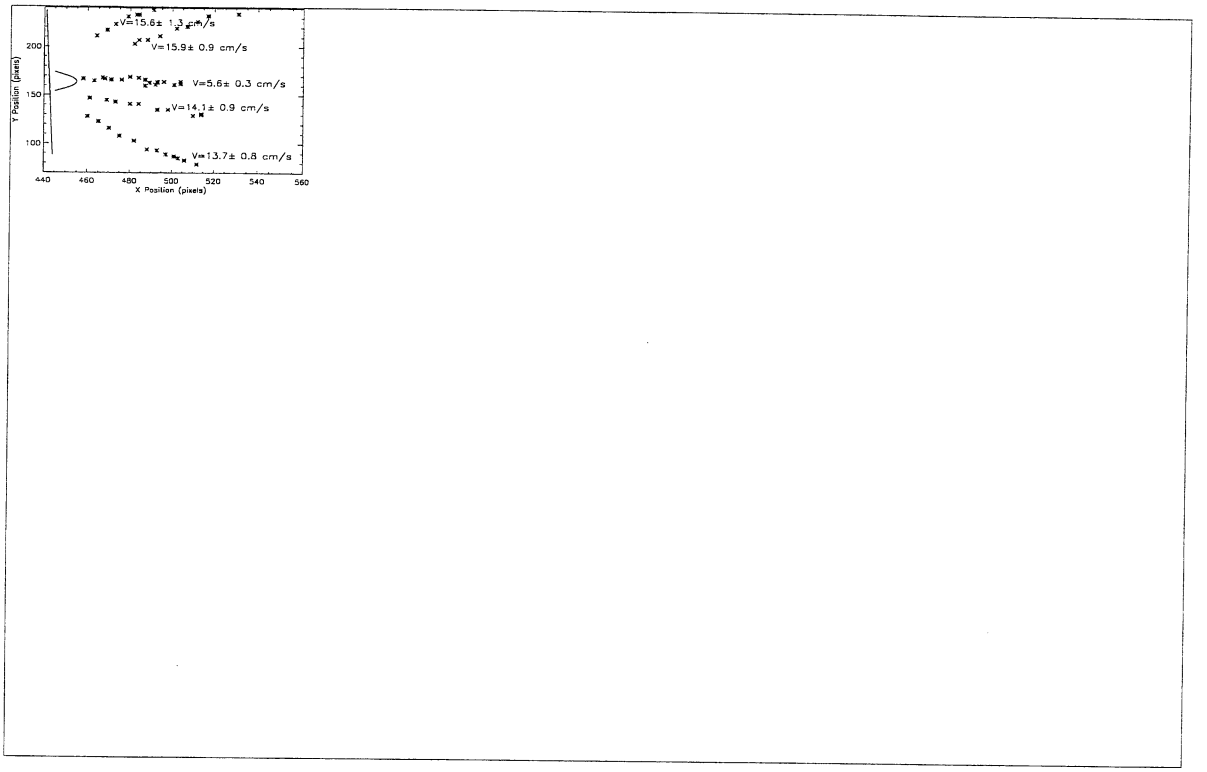

Figure 8: The target surface and impact site (left) for IBS 4 are plotted with the trajectories of five points along the ejecta curtain and the derived speeds for those points.

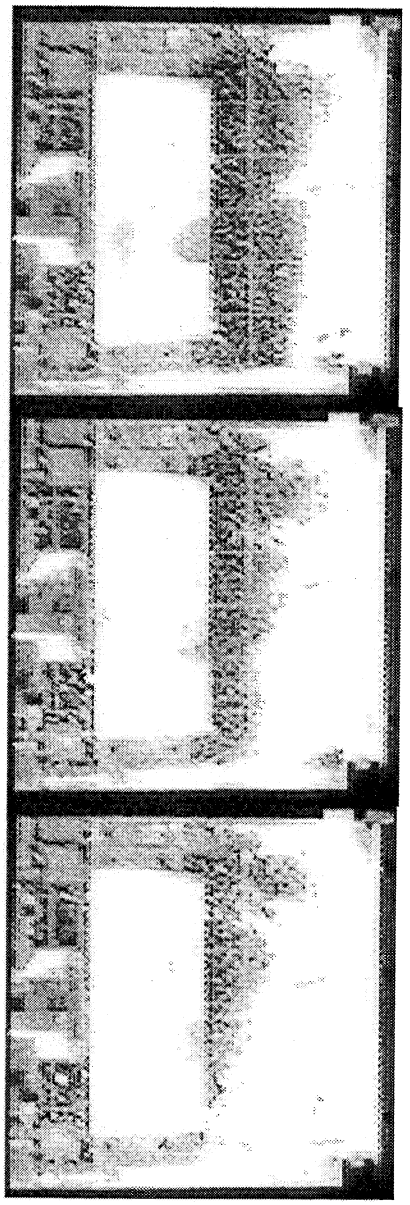

Figure 9: Three frame sequence at 0.5 second intervals from the impact in IBS 6 at 28 cm/s. The impact was slightly oblique (Table 2) leading to the asymmetric ejecta distribution seen here.